

Spin structure of the nucleon: QCD evolution, lattice results and models

M. Altenbuchinger^{1a}, Ph. Hägler^{1,2b}, W. Weise^{1c}, and E. M. Henley³

¹ Physik Department, Technische Universität München, D-85747 Garching, Germany

² Institut für Theoretische Physik, Universität Regensburg, D-93040 Regensburg, Germany

³ Dept. of Physics, University of Washington, Seattle, WA 98195-1560, USA

Received: date / Revised version: date

Abstract The question how the spin of the nucleon is distributed among its quark and gluon constituents is still a subject of intense investigations. Lattice QCD has progressed to provide information about spin fractions and orbital angular momentum contributions for up- and down-quarks in the proton, at a typical scale $\mu^2 \sim 4 \text{ GeV}^2$. On the other hand, chiral quark models have traditionally been used for orientation at low momentum scales. In the comparison of such model calculations with experiment or lattice QCD, fixing the model scale and the treatment of scale evolution are essential. In this paper, we present a refined model calculation and a QCD evolution of lattice results up to next-to-next-to-leading order. We compare this approach with the Myhrer-Thomas scenario for resolving the proton spin puzzle.

PACS. 14.20.Dh Protons and neutrons – 12.39.Ba Bag model – 12.38.Bx Perturbative calculations

1 Introduction

How is the total spin $1/2$ of the nucleon distributed among its quark and gluon constituents? This question has been intensely discussed ever since the EMC experiment presented first results for the spin asymmetry in polarized muon proton scattering in 1987 [1]. This measurement indicated that only about 15% or less of the nucleon spin is built up by quark spins, although with sizeable statistical and systematic uncertainties. More recent measurements of HERMES and COMPASS [2, 3] and their QCD analysis [4–6] showed that the nucleon receives still only about one third of its spin from quark spins:

$$\Delta\Sigma_{\text{HERMES}}(5 \text{ GeV}^2) = 0.330 \pm 0.011_{\text{theo.}} \pm 0.025_{\text{exp.}} \pm 0.028_{\text{evol.}}, \quad (1)$$

determined at a scale $\mu^2 = 5 \text{ GeV}^2$. This is in stark contrast to naive model calculations, as for example in the non-relativistic quark model that suggests $\Delta\Sigma = 1$. Relativistic effects reduce $\Delta\Sigma$ to about two thirds, still far too large in comparison with Eq. (1). Myhrer and Thomas proposed in [7–10] that $\Delta\Sigma$ could be further reduced by

including pion cloud contributions and corrections from one gluon exchanges. With such corrections they end up with a result for $\Delta\Sigma$ that is consistent with experiment. The missing $\approx 60 - 70\%$ of the nucleon spin reappear entirely as orbital angular momentum of up and down quarks. On the other hand, L_{u+d} , appears to be in strong contrast to lattice calculations [11–13] where the orbital angular momentum contribution L_{u+d} comes out close to zero [13]. To explain this difference, Thomas [8] proposed to consider the renormalization scale (μ -)dependence of the quantities appearing in the nucleon spin sum rule [14]

$$\frac{1}{2} \Delta\Sigma + L_q + L_g + \Delta G = \frac{1}{2}, \quad (2)$$

defined by the following expectation values taken for a spin-up state of the proton, $|P+\rangle$:

$$\begin{aligned} \Delta\Sigma &= \langle P+ | \int d^3x \bar{\psi} \gamma^3 \gamma_5 \psi | P+ \rangle, \\ \Delta G &= \langle P+ | \int d^3x (E^1 A^2 - E^2 A^1) | P+ \rangle, \\ L_q &= \langle P+ | i \int d^3x \psi^\dagger (x^1 \partial^2 - x^2 \partial^1) \psi | P+ \rangle, \\ L_g &= \langle P+ | \int d^3x E^i (x^2 \partial^1 - x^1 \partial^2) A^i | P+ \rangle. \end{aligned} \quad (3)$$

^a altenb@ph.tum.de

^b phaegler@ph.tum.de

^c weise@ph.tum.de

Here ψ is the quark field, E^i and A^μ are the gluon electric field and gauge potential. A sum over quark flavors is implicit in the definition of the flavor singlet quantities in Eq. (3). Contributions in the non-singlet sector will be denoted by $\Delta\Sigma_{u-d}$, L_{u-d} etc. . The L_g is the orbital angular momentum contribution from gluons and ΔG is the gluon spin part. It is important to note that L_q , L_g and ΔG in Eq. (3) are not explicitly gauge invariant. A manifestly gauge invariant decomposition and its relation to moments of generalized parton distributions was presented by Ji in [15, 16]:

$$\frac{1}{2}\Delta\Sigma + L_q^{\text{GI}} + J_g^{\text{GI}} = \frac{1}{2}, \quad (4)$$

where $\Delta\Sigma$ is given as before, L_q^{GI} is obtained from L_q replacing ∂^μ by the gauge-covariant derivative, $\partial^\mu \rightarrow D^\mu$, and the total gluon angular momentum is defined as

$$J_g^{\text{GI}} = \langle P + | \int d^3x [\mathbf{x} \times (\mathbf{E} \times \mathbf{B})]_3 | P + \rangle. \quad (5)$$

Using a leading order QCD evolution of the spin contributions from the low, hadronic model scale to the higher scale of the lattice results, it was shown in Ref. [8] that it is possible to find at least a qualitative agreement with the lattice data.

With these previous achievements in mind, the purpose of the present work is twofold: first, we extend the QCD evolution to next-to-leading (NLO) and next-to-next-to-leading (NNLO) order and perform a backwards evolution starting from lattice results. This approach has the advantage that the scale dependence of the spin contributions is rather weak at the higher scale of lattice results, and that the extrapolation therefore does not suffer from the uncertainty of the slope in μ at low scales. Most importantly, proceeding in this way we do not have to fix the model scale a priori, which is generically difficult, but have the possibility to compare model results over a wider range of low scales with the downward-evolved lattice data. As a further extension, we use not only the perturbative coupling $\alpha_s(\mu)$ in the evolution equations but employ also a frequently suggested “non-perturbative” strong coupling that approaches a constant $\alpha_{s,\text{max}}^{\text{eff}}$ in the infrared region.

The second purpose of this work is to reexamine the model calculations of [7–10] and also to study possible improvements (Section 3). Given these results and the evolved lattice data, we conclude with a discussion in Section 4.

2 QCD evolution of lattice results

In this section our aim is to evolve results from lattice QCD, usually provided in the $\overline{\text{MS}}$ scheme at a scale $\mu^2 \simeq 4 \text{ GeV}^2$, down to the low scales characteristic of model calculations. The lattice calculations were performed on the basis of manifestly gauge invariant operators. The computations correspond to the spin decomposition proposed by Ji, Eq. (4). For the remainder of this section, we will

therefore employ the gauge invariant definitions of the spin observables. We drop the superscript GI in the following for better readability. To obtain the complete set of evolution equations for all individual parts of the spin sum rule, we define the orbital angular momentum of quarks as $L_q = J_q - \frac{1}{2}\Delta\Sigma$, of gluons as $L_g = J_g - \Delta G$ (for discussions of the latter definition, see Refs. [16–18]).

Note that the gauge invariant ΔG cannot be represented in terms of a local operator [19], but it can be defined as the lowest x -moment of the gauge invariant gluon spin distribution, $\Delta g(x)$. Despite remarkable experimental and theoretical efforts with respect to polarized parton distributions [4–6, 20–22], little is known so far about the magnitude of ΔG . Concerning the numerical evaluation of the evolution equations, we will therefore concentrate on the quark spin, the quark orbital angular momentum and the total angular momentum of the gluons. As will be shown below, this can be done without explicit knowledge about ΔG and $L_g = J_g - \Delta G$. It then follows that the evolution of all quantities of interest can also be performed at NNLO, employing known results for the relevant anomalous dimensions from the literature.

The total angular momentum contributions J_q and J_g are introduced as in [16] in the framework of generalized parton distributions. We observe that J_q and J_g mix in exactly the same way under renormalization as the (symmetric and traceless) quark and gluon energy momentum tensors. This can be seen for example by rewriting

$$\begin{aligned} \langle P, s | J_{q,g}^i | P, s \rangle = & \\ \frac{1}{2} \epsilon^{ijk} \lim_{\Delta^\mu \rightarrow 0} \left[i \frac{\partial}{\partial \Delta^j} \langle P + \frac{\Delta}{2}, s | T_{q,g}^{0k} | P - \frac{\Delta}{2}, s \rangle \right. & \\ \left. - i \frac{\partial}{\partial \Delta^k} \langle P + \frac{\Delta}{2}, s | T_{q,g}^{0j} | P - \frac{\Delta}{2}, s \rangle \right] (2\pi)^3 \delta(\Delta), & \quad (6) \end{aligned}$$

where P is the quark momentum, s the quark helicity, and Δ is a momentum difference between incoming and outgoing quark. Here, the additional derivative with respect to the momentum transfer, Δ^μ , cannot have any influence on the singular behavior of the operators. Therefore they mix in the same manner. The QCD evolution equations for J_q and J_g are constructed using the spin-2 singlet anomalous dimension given at next-to-leading order in [23, 24] and at next-to-next-to-leading order in [25–27]. This yields

$$\begin{aligned} \frac{d}{d \ln \mu^2} \begin{pmatrix} J_q \\ J_g \end{pmatrix} = -\frac{\alpha_s}{4\pi} \begin{pmatrix} \frac{32}{9} & -\frac{2}{3}n_F \\ -\frac{32}{9} & \frac{2}{3}n_F \end{pmatrix} \begin{pmatrix} J_q \\ J_g \end{pmatrix} \\ - \left(\frac{\alpha_s}{4\pi} \right)^2 \begin{pmatrix} a_1 - b_1 n_F & -d_1 n_F \\ -a_1 + b_1 n_F & d_1 n_F \end{pmatrix} \begin{pmatrix} J_q \\ J_g \end{pmatrix} \\ - \left(\frac{\alpha_s}{4\pi} \right)^3 \begin{pmatrix} a_2 - b_2 n_F - c_2 n_F^2 & -d_2 n_F + e_2 n_F^2 \\ -a_2 + b_2 n_F + c_2 n_F^2 & d_2 n_F - e_2 n_F^2 \end{pmatrix} \begin{pmatrix} J_q \\ J_g \end{pmatrix} \end{aligned} \quad (7)$$

for n_F flavours (compare also [28]), with entries a_i, b_i, \dots given in Table 1. For the non-singlet combination J_q^{NS} , we find Eq. (8). The evolution equations for the spin contributions at NNLO in the $\overline{\text{MS}}(\overline{\text{MS}})$ scheme [29, 30] (these

Table 1. Coefficients entering the evolution equations (7).

a_1	b_1	d_1	a_2	b_2	c_2	d_2	e_2
$\frac{11744}{243}$	$\frac{416}{81}$	$\frac{611}{81}$	$\frac{5514208}{6561} + \frac{1280}{81}\zeta(3)$	$\frac{134888}{2187} + \frac{2560}{27}\zeta(3)$	$\frac{1136}{243}$	$\frac{670871}{4374} - \frac{2600}{27}\zeta(3)$	$\frac{8830}{729}$

$$\begin{aligned} \frac{d}{d \ln \mu^2} J_q^{NS} = & -\frac{\alpha_s}{4\pi} \frac{32}{9} J_q^{NS} - \left(\frac{\alpha_s}{4\pi}\right)^2 \left(\frac{11744}{243} - \frac{256}{81} n_F\right) J_q^{NS} \\ & - \left(\frac{\alpha_s}{4\pi}\right)^3 \left(\frac{5514208}{6561} + \frac{1280}{81} \zeta(3) - \frac{167200}{2187} n_F - \frac{1280}{27} n_F \zeta(3) - \frac{896}{729} n_F^2\right) J_q^{NS}. \end{aligned} \quad (8)$$

two schemes are simply connected through a change in the renormalization scale) are given by [31–33]

$$\begin{aligned} \frac{d}{d \ln \mu^2} \begin{pmatrix} \Delta\Sigma \\ \Delta G \end{pmatrix} = & -\frac{\alpha_s}{4\pi} \begin{pmatrix} 0 & 0 \\ -4 & -\beta_0 \end{pmatrix} \begin{pmatrix} \Delta\Sigma \\ \Delta G \end{pmatrix} \\ & - \left(\frac{\alpha_s}{4\pi}\right)^2 \begin{pmatrix} 8n_F & 0 \\ -\frac{236}{3} + \frac{8}{9}n_F & -\beta_1 \end{pmatrix} \begin{pmatrix} \Delta\Sigma \\ \Delta G \end{pmatrix} \\ & - \left(\frac{\alpha_s}{4\pi}\right)^3 \begin{pmatrix} \frac{472}{3}n_F - \frac{16n_F^2}{9} & 0 \\ \gamma_{gq} & \gamma_{gg} \end{pmatrix} \begin{pmatrix} \Delta\Sigma \\ \Delta G \end{pmatrix}. \end{aligned} \quad (9)$$

At NNLO, the anomalous dimensions γ_{gq} and γ_{gg} are still unknown, while the upper row (γ_{qq}, γ_{qg}) has been obtained as described in [33]. Here the QCD beta functions are

$$\beta_0 = 11 - \frac{2n_F}{3}, \quad \beta_1 = 102 - \frac{38}{3}n_F. \quad (10)$$

We emphasize that in the chosen renormalization scheme, the evolution of $\Delta\Sigma$ is independent of ΔG , even at NNLO. Furthermore, since $J_q + J_g = 1/2$ at any scale, the evolution of J_q does not require an independent knowledge of the value of J_g . Hence one finds the remarkable result, already mentioned above, that neither ΔG nor $L_g = J_g - \Delta G$ are actually required in practice for the scale evolution of $L_q = J_q - \Delta\Sigma/2$. As a consequence the evolution of all the quantities in Eq. (4) can be performed at NNLO.

Employing the definitions of L_q and L_g given above, fully consistent coupled evolution equations for the orbital angular momenta of quarks and of gluons can be written,

$$\begin{aligned} \frac{d}{d \ln \mu^2} \begin{pmatrix} L_q \\ L_g \end{pmatrix} = & -\frac{\alpha_s}{4\pi} \begin{pmatrix} \frac{32}{9} & -\frac{2}{3}n_F \\ -\frac{32}{9} & \frac{2}{3}n_F \end{pmatrix} \begin{pmatrix} L_q \\ L_g \end{pmatrix} \\ & - \frac{\alpha_s}{4\pi} \begin{pmatrix} \frac{16}{9} & -\frac{2}{3}n_F \\ \frac{20}{9} & 11 \end{pmatrix} \begin{pmatrix} \Delta\Sigma \\ \Delta G \end{pmatrix} \\ & - \left(\frac{\alpha_s}{4\pi}\right)^2 \begin{pmatrix} \frac{11744}{243} - \frac{416}{81}n_F & -\frac{611}{81}n_F \\ -\frac{11744}{243} + \frac{416}{81}n_F & \frac{611}{81}n_F \end{pmatrix} \begin{pmatrix} L_q \\ L_g \end{pmatrix} \\ & - \left(\frac{\alpha_s}{4\pi}\right)^2 \begin{pmatrix} \frac{5872}{243} - \frac{532}{81}n_F & -\frac{611}{81}n_F \\ \frac{13244}{243} + \frac{136}{81}n_F & 102 - \frac{415}{81}n_F \end{pmatrix} \begin{pmatrix} \Delta\Sigma \\ \Delta G \end{pmatrix}, \end{aligned} \quad (11)$$

Table 2. Lattice QCD results from Ref. [35] for $\Delta\Sigma/2$ and L_q in the $\overline{\text{MS}}$ scheme at $\mu^2 = 4 \text{ GeV}^2$, separated into u- and d-quark contributions. Statistical and estimated systematic uncertainties due to the renormalization are given in the form $(\dots)_{\text{stat}}(\dots)_{\text{ren}}$.

	$\Delta\Sigma/2$	L_q
u	0.411(36)	-0.175(36)(17)
d	-0.203(35)	0.205(35)(0)

at next-to-leading order in the $\overline{\text{MS}}$ scheme.

An overview of lattice QCD calculations of nucleon spin observables, in particular of moments of generalized parton distributions that give access to the total quark angular momentum J_q , can be found in [34]. Here we focus on the latest published results from the LHP collaboration [35]. They were obtained in the framework of a mixed action approach with $n_F = 2+1$ dynamical fermions, with lattice pion masses as low as $\approx 300 \text{ MeV}$. The computationally demanding quark line disconnected diagrams, which contribute in the singlet sector, were not included in this study. The final values for $\Delta\Sigma_q$, L_q and J_q at the physical pion mass were obtained from extrapolations employing the covariant baryon chiral perturbation theory results of [36]. We refer to the original publication [35] for the details of the lattice simulation, the numerical analysis, and a discussion of the statistical and systematic uncertainties. A summary of the lattice results, for the $\overline{\text{MS}}$ scheme at a scale of 4 GeV^2 , is given in Table 2. The errors given in this table do not include systematic uncertainties from chiral extrapolations and disconnected diagrams.

For our QCD evolution of lattice results, we assume a vanishing contribution from strange quarks (see also [37]). The total gluon angular momentum is given by $J_g = \frac{1}{2} - J_{u+d}$. As starting values at $\mu^2 = 4 \text{ GeV}^2$, we use the numbers given in Table 2. For the running coupling, we set $\alpha_s^{\text{NNLO}, n_F=5}(M_Z) = 0.1184$ [38], and employ the flavor matching conditions [39, 40] to obtain $\Lambda_{\text{QCD}}^{\text{NNLO}, n_F=3} = 0.338 \text{ GeV}$, $\Lambda_{\text{QCD}}^{\text{NLO}, n_F=3} = 0.388 \text{ GeV}$, and $\Lambda_{\text{QCD}}^{\text{LO}, n_F=3} = 0.148 \text{ GeV}$. With this input, we have solved the LO, NLO and NNLO coupled evolution equations and found the scale dependence plotted in Figures 1 and 2.

The results at LO, NLO and NNLO, employing the standard analytical expressions for the perturbative strong coupling constant (corresponding to an expansion in

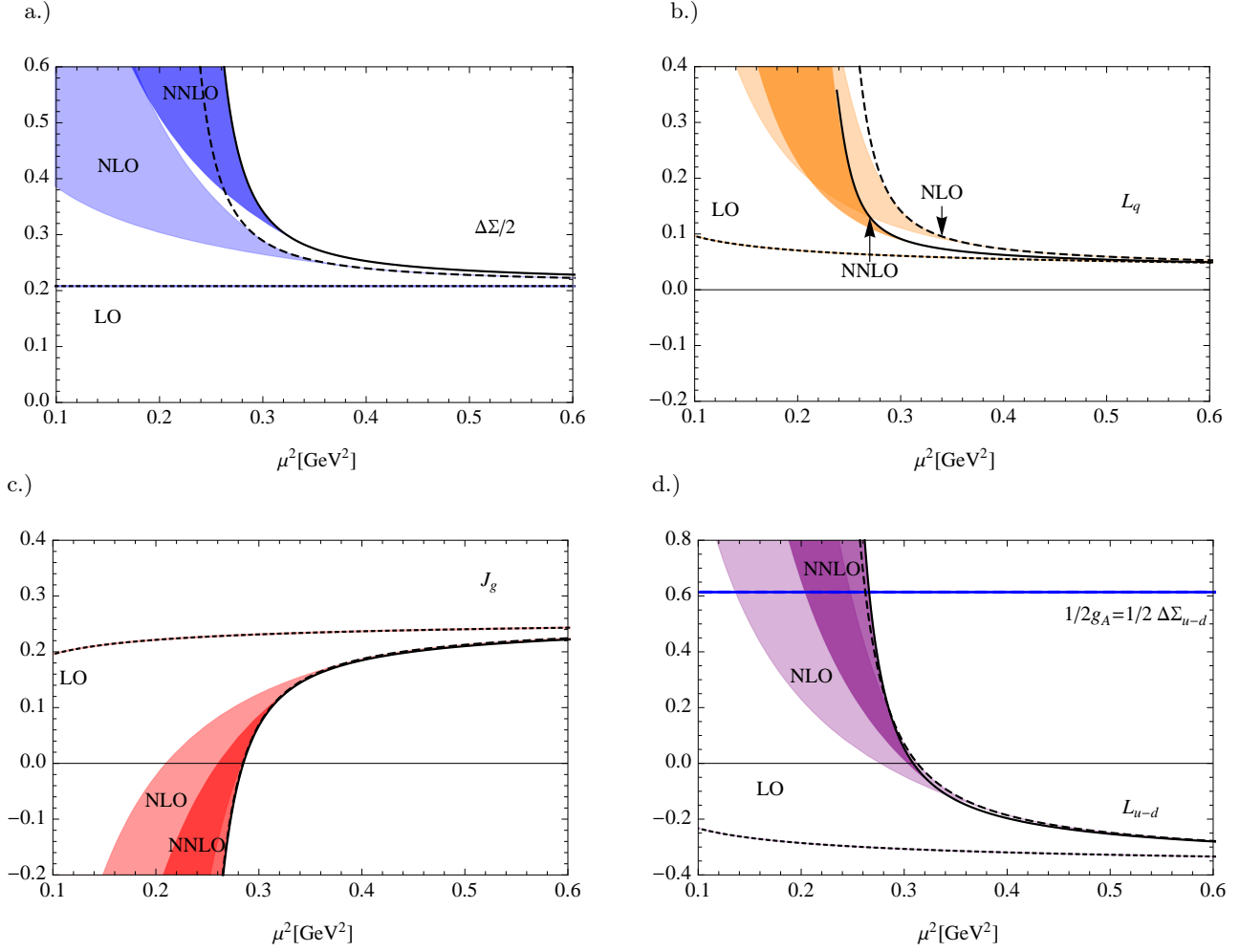


Figure 1. Scale dependence of $\Delta\Sigma/2$, L_q , J_g , and L_{u-d} shown together with $\frac{1}{2}g_A = \frac{1}{2}\Delta\Sigma_{u-d}$, starting from the lattice QCD results at $\mu^2 = 4 \text{ GeV}^2$ given in Table 2. In all diagrams the solid, dashed and short-dashed black lines are solutions of the QCD evolution equations at NNLO, NLO, and LO, respectively. The colored bands are obtained by imposing upper bounds for α_s (see text).

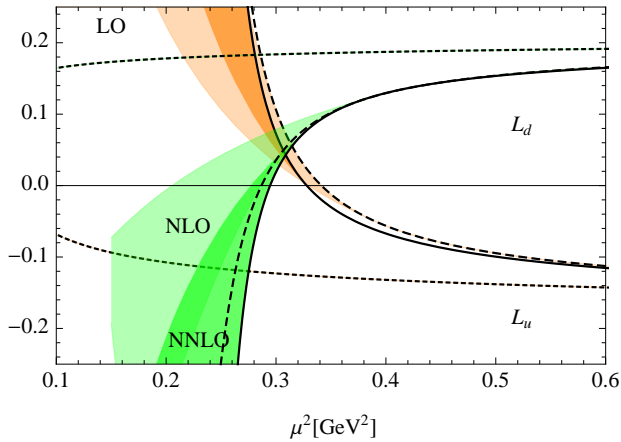


Figure 2. Evolution of L_u and L_d in NNLO (solid lines), NLO (dashed lines) and LO (short dashed lines). The shaded areas are assigned as in Fig. 1.

$1/\ln(\mu^2/\Lambda^2)$ beyond LO, see, e.g., [38]) in the $\overline{\text{MS}}$ scheme at the appropriate order, are given by the short-dashed, dashed, and solid black curves, respectively. We note that the deviation of the approximate analytical expressions for α_s from the exact (numerical) solutions of the evolution equations increases as one approaches lower scales. For $n_F = 3$ and $\Lambda_{\text{QCD}}^{\text{NNLO}, n_F=3} = 0.338 \text{ GeV}$, the formally exact solution for the running coupling at NNLO would already diverge around $\mu^2 \sim 0.27 \text{ GeV}^2$. The curves in Fig. 1 obtained for α_s in the $1/\ln(\mu^2/\Lambda^2)$ -approximation are therefore only indicative for a strong coupling constant that grows indefinitely as $\mu^2 \rightarrow 0$.

A comparison with the model results, e.g. as proposed by Myhrer and Thomas [7–10], requires an evolution down to scales $\mu^2 \sim 0.1 - 0.3 \text{ GeV}^2$, far away from the perturbative QCD regime. From the results in Figs. 1 and 2, we find that the evolution curves at NLO and NNLO begin to show a very strong curvature exactly in this region. Clearly, at such low scales quantitative statements based

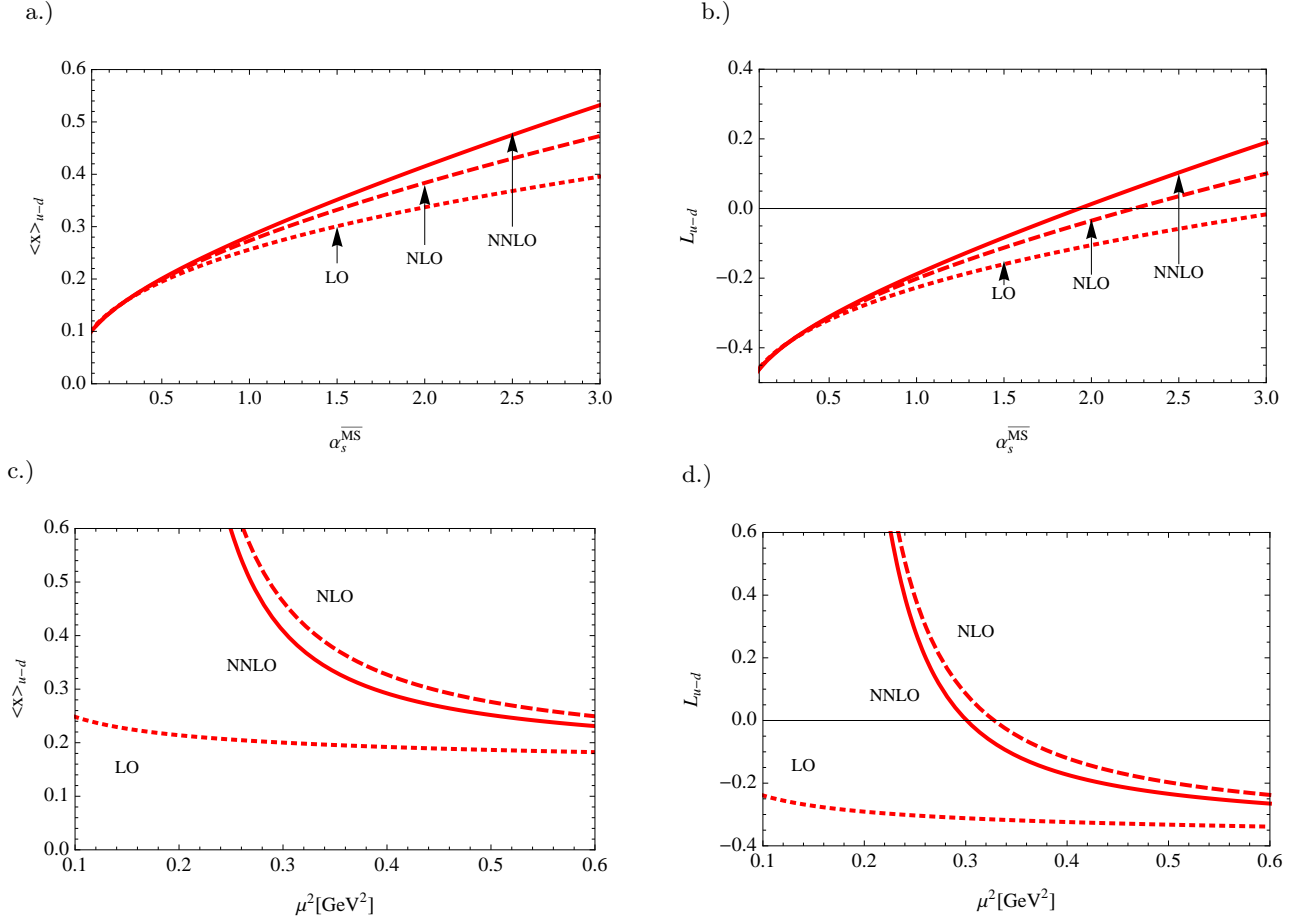


Figure 3. α_s -dependence of the momentum and angular momentum contributions $\langle x \rangle_{u-d}$ and L_{u-d} with starting values fixed at $\alpha_{s,0} = 0.28$. Diagrams c and d show the corresponding renormalization scale dependence. In all the diagrams solid, dashed and short-dashed red lines correspond to NNLO, NLO, and LO, respectively.

on a perturbative QCD analysis (including the running of α_s) are no longer reliable.

With respect to (the non-perturbative) α_s , one would expect in any case that it saturates at low scales, as suggested by non-perturbative resummation in the infrared region [41–43]. A further rough impression about the uncertainties in the evolution may therefore be obtained as follows. As an alternative to the infrared divergent, perturbative coupling $\alpha_s(\mu^2)$ in the evolution equations, we consider an effective $\alpha_s^{\text{eff}}(\mu)$ that approaches a fixed value $\alpha_{s,\text{max}}^{\text{eff}}$ at small μ^2 . For the corresponding numerical calculation we use $\alpha_s^{\text{eff}}(\mu^2) = \alpha_s(\mu^2)$ of appropriate order in the $\overline{\text{MS}}$ scheme for all μ for which $\alpha_s(\mu^2) \leq \alpha_{s,\text{max}}^{\text{eff}}$. Below the scale μ_0 at which $\alpha_s(\mu_0^2) = \alpha_{s,\text{max}}^{\text{eff}}$, we use $\alpha_s^{\text{eff}} \equiv \alpha_{s,\text{max}}^{\text{eff}}$. For illustration, we chose two different values, $\alpha_{s,\text{max}}^{\text{eff}} = 1.5$ and $\alpha_{s,\text{max}}^{\text{eff}} = 3$. Performing the evolution with these restricted couplings spans the shaded colored bands in Figures 1 and 2. The boundary with flatter evolution always corresponds to $\alpha_{s,\text{max}}^{\text{eff}} = 1.5$, the steeper one to $\alpha_{s,\text{max}}^{\text{eff}} = 3$. The lighter colored bands correspond to NLO, the darker colored bands to NNLO. The relatively small $\Lambda_{\text{QCD}}^{\text{LO}, n_F=3} = 0.148 \text{ GeV}$, obtained from the flavor matching procedure, implies that the correspond-

ing $\alpha_s(\mu^2)$ at LO stays below $\alpha_{s,\text{max}}^{\text{eff}}$ in the considered region of μ^2 . Hence no bands are shown in this case, and one finds the remarkably stable (but unrealistic) LO evolution shown in the figures.

NLO and NNLO evolution results in the dashed and solid lines, and the lighter and darker shaded colored bands, respectively. As mentioned before, in contrast to the LO evolution, strong evolution effects can already be seen at scales $\mu^2 \lesssim 0.3 \text{ GeV}^2$. Before discussing the results in more detail, we note as a general feature that the bands obtained for our choices of $\alpha_{s,\text{max}}^{\text{eff}}$ start to broaden quickly below $\mu^2 \sim 0.3 \text{ GeV}^2$, indicating potentially large uncertainties in the evolution as one enters the non-perturbative regime. With the exception of $\Delta\Sigma$, we observe a broad overlap of the NLO and NNLO bands for each of the different observables.

At these orders we find interesting qualitative and quantitative changes of the proton spin decomposition under evolution. The singlet quark spin contribution $\Delta\Sigma$ becomes scale dependent at NLO and increases with lower scales, a behavior that is even more strongly pronounced in NNLO. Similarly, the contribution from L_q stays positive and grows quickly at low scales, while J_g crosses zero

in the region of $\mu^2 \sim 0.21$ to 0.29 GeV^2 and then becomes large and negative. At the same time, L_{u-d} ¹ shows a strong upwards bending and moves from its negative starting value at higher scales towards large positive values at low scales, crossing zero around $\mu^2 \sim 0.28$ to 0.32 GeV^2 . From the evolution of L_q and L_{u-d} one can deduce the separate μ -dependences of L_u and L_d , as displayed in Figure 2. Both L_u and L_d change sign under evolution. As one moves in the direction of lower scales, the contribution from the up-quarks, L_u , changes from negative to increasingly large positive values at about $\mu^2 \sim 0.32 - 0.35 \text{ GeV}^2$, while the zero crossing of L_d from positive to increasingly large negative values takes place at slightly lower scales of $\mu^2 \sim 0.2$ to 0.3 GeV^2 . Similar trends have already been observed in the LO-study of Ref. [8], based however on a substantially larger $\Lambda_{\text{QCD}}^{\text{LO,nf}=3} = 0.24 \text{ GeV}$. It is interesting to observe that the crossing points of L_u and L_d roughly match as we proceed from NLO to NNLO.

For a better understanding of the scale dependence at very low scales, i.e. for large values of the strong coupling constant, it is instructive to present the evolution in terms of α_s instead of μ .² This is illustrated in Figure 3 for the nucleon isovector momentum fraction $\langle x \rangle_{u-d}$ on the left and for L_{u-d} on the right. Note that the evolution equations for both quantities are based on the same anomalous dimension. The results were obtained by rewriting the evolution equations, i.e. translating derivatives with respect to μ^2 into derivatives with respect to α_s , and then replacing $\frac{d\alpha_s}{d \ln \mu^2}$ by the QCD β -function. As starting values we have used $\langle x \rangle_{u-d} = 0.155$ and $L_{u-d} = -0.38$ [35] at $\alpha_{s,0} = 0.28$ (corresponding to a scale of $\mu^2 \sim 4 \text{ GeV}^2$). Both quantities are remarkably stable under evolution in α_s , even at large α_s . For example, at $\alpha_s = 2.0$ the momentum fraction $\langle x \rangle_{u-d}$ at NLO is about $\sim 14\%$ larger than the LO result, and NNLO and NLO results differ by only about $\sim 8\%$. Apart from the difference in the starting values, the form of the α_s -dependence is identical for L_{u-d} and $\langle x \rangle_{u-d}$. The zero crossing of L_{u-d} quickly moves to smaller α_s as the order of the perturbative evolution is increased. Figures 3c and d show how the α_s dependences translate to a renormalization scale dependence. The logarithmic dependence of $\alpha_s(\mu)$ that shows up strongly as μ approaches Λ_{QCD} , produces the strong curvature in the evolution of the observables as functions of the scale μ .

Small but unimportant differences between Fig. 3d and Fig. 1d result from the slightly different procedures involved, as described.

Further remarks on the evolution and a comparison of evolved lattice results with calculations performed in a chiral quark model will be presented below in Section 4.

¹ showing less systematic uncertainties in the lattice computation as contributions from disconnected diagrams cancel out for isovector quantities

² Ph.H. would like to thank M. Diehl for helpful discussions on this point.

3 Contributions to the nucleon spin in a chiral quark model

3.1 Pion cloud contributions, revisited

It is a well established fact that the nucleon is a complex many-body system, with the three valence quarks and multiple quark-antiquark pairs embedded in a strong, non-perturbative gluonic field configuration. Chiral quark models draw a simplified picture of this complexity in terms of valence quarks in a confining bag coupled to the pion cloud, based on spontaneously broken chiral symmetry in low-energy QCD. A frequently used representative of such chiral models is the cloudy bag (CBM) [44–46] that couples the pion cloud to quarks in the MIT bag [47] such that chiral invariance is realized in the limit of massless quarks. This section summarizes the present status concerning nucleon spin structure from this model point of view.

The relativistic treatment of quarks itself yields already results that differ significantly from the ordinary SU(6) quark model predictions. The $\Delta\Sigma = 1$ of the non-relativistic quark model is reduced to about $\Delta\Sigma^{\text{MIT}} = 0.65$ in the MIT bag model. The “missing spin” is interpreted as orbital angular momentum of the valence quarks, $2L_{u+d}^{\text{MIT}} = 0.35$, associated with the lower components of the Dirac quark wave functions.

The correction factors for the pion cloud in the CBM were already derived by Myhrer and Thomas in [7–10]. For the singlet expectation values,

$$\Delta\Sigma^{\text{CBM}} = 0.65 \cdot \Pi_S(R), \quad 2L_q^{\text{CBM}} = 0.35 \cdot \Pi_S(R), \\ 2L_\pi^{\text{CBM}} = 1 - \Pi_S(R), \quad (12)$$

and for the non-singlet expectation values [37],

$$\Delta\Sigma_{u-d}^{\text{CBM}} = g_A^{(3)\text{CBM}} = \frac{5}{3} \cdot 0.65 \cdot \Pi_{\text{NS}}(R), \\ 2L_{u-d}^{\text{CBM}} = \frac{5}{3} \cdot 0.35 \cdot \Pi_{\text{NS}}(R). \quad (13)$$

We have denoted the pion cloud correction factors by $\Pi_S(R)$ and $\Pi_{\text{NS}}(R)$, each for a given bag radius R . For their explicit form we refer to [7–10, 37] and references therein. We have reproduced these factors using the formalism described in [46]. Their radius dependence is plotted in Figure 4. The singlet correction factor, Π_S , is smaller than unity and hence leads to the expected reduction of the quark spin contribution. At the same time, $\Pi_{\text{NS}} < 1$ leads to a slightly less favourable comparison of $g_A^{(3)\text{CBM}}$ with the experimental value of g_A . This mismatch is a feature that depends on the chiral representation chosen for the model. In particular, as pointed out in [37], choosing a volume coupling version instead of the standard surface coupling reproduces the experimental value of $g_A^{(3)}$ with very good accuracy. A common way of treating the discrepancy between $g_A^{(3)\text{CBM}}$ and the empirical $g_A \equiv g_A^{(3)} = 1.27$ is by inclusion of a phenomenological

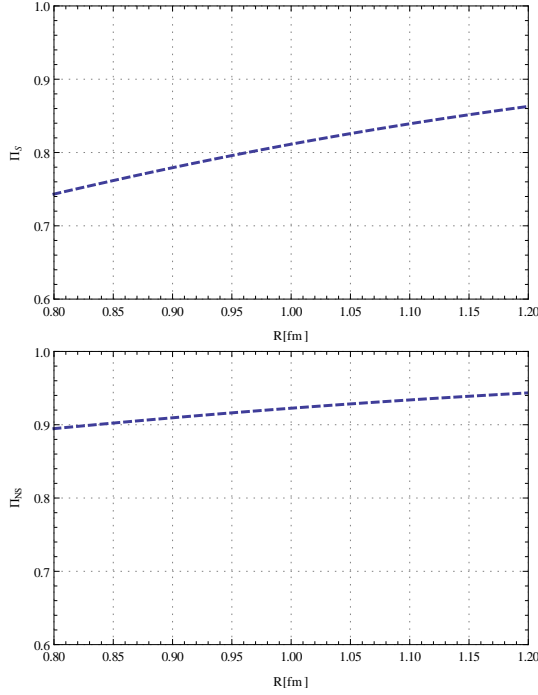


Figure 4. Radius dependence of the singlet and non-singlet corrections Π_S and Π_{NS} associated with the pion cloud of the nucleon.

center-of-mass correction. This correction is just a multiplicative factor for $\Delta\Sigma$ and $\Delta\Sigma_{u-d}$.³ For consistency, however, one should then also rescale L_q and L_{u-d} accordingly to keep the spin sum rule conserved. The corresponding results are shown in Table 3, in addition to results obtained without the center-of-mass corrections. If explicit gluon operators are taken into account (see Table 4 and section 3.2 below), these corrections cannot be applied uniquely. In that case we give only the model results without rescaling by c.m. corrections.

A detailed analysis of $\Delta\Sigma$ also requires, in principle, a discussion of $g_A^{(8)}$ since the flavour singlet axial vector coupling constant extracted from polarised deep inelastic scattering is sensitive to that value. In the present case we restrict ourselves to a flavor-SU(2) cloudy bag model which implies $\Delta\Sigma = g_A^{(8)}$. This is quite compatible with the small strange quark contribution $\Delta s \sim -0.01$ discussed in Ref. [37].

3.2 Corrections from one-gluon exchange processes

The MIT bag model produces degenerate masses of the nucleon and the delta, whereas the empirical mass splitting is about 300 MeV. In order to account for this mass difference, an additional spin-spin interaction between quarks is introduced. The traditional ad-hoc way of doing this

³ Notice that the value $g_A^{(3)} = 1.27$, given in [7–10], is obtained by adjusting the phenomenological center-of-mass correction, while this correction has not been included for any of the other spin observables listed in these references.

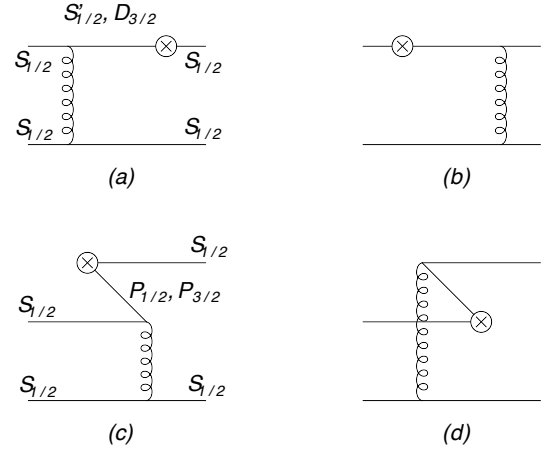


Figure 5. One-gluon exchange (OGE) corrections for $\Delta\Sigma$, $L_{S,NS}$ and $g_A^{(3)}$. Diagram (a) and (b) are contribution from intermediate quark states and (c) and (d) from quark-antiquark pairs.

is by allowing one-gluon exchanges between quarks in the interior of the bag, with an effective coupling $\tilde{\alpha}_s$. This coupling should not be confused with the strong coupling of QCD. It represents a free parameter chosen in such a way that the model reproduces the light hadron spectrum [48]. The values used in the literature vary between $\tilde{\alpha}_s = 1$ [49] and $\tilde{\alpha}_s = 2.2$ [50]. We use these two values as options in the results shown later in Table 3 and 4.

We have performed calculations in analogy to Ref. [50], where the color magnetic corrections to baryon magnetic moments and to semileptonic decays, i.e. the axial coupling constant, were derived at order $\tilde{\alpha}_s$. Following the arguments given there, we neglect the color electric corrections and drop loop diagrams. That means, we consider diagrams 5(a)-5(d), in which only color magnetic gluons are exchanged.

For the singlet expectation values, $\Delta\Sigma$ and L_q , we find the (additive) OGE corrections

$$\delta\Delta\Sigma = -2\delta_g \cdot \tilde{\alpha}_s, \quad \delta L_q = \delta_g \cdot \tilde{\alpha}_s, \quad (14)$$

with $\delta_g \simeq 2.5 \cdot 10^{-2}$, where L_q is used in its non-gauge-invariant formulation (3), and intermediate (anti-)quarks in the orbitals $P_{1/2}, P_{3/2}, D_{3/2}, S'_{1/2}, P'_{1/2}, P'_{3/2}, D'_{3/2}, S''_{1/2}$ are taken into account (conventions are chosen as in [50]). As already pointed out in [7–10] the corrections are mainly due to antiquarks propagating in the $P_{1/2}, P_{3/2}$ orbitals. Compared to $\delta\Delta\Sigma \sim -0.15$ and $\delta L_q \sim 0.08$ for $\tilde{\alpha}_s = 2.2$ as presented in [8, 9], our corrections are slightly smaller.

For the non-singlet operators we find:

$$\delta\Delta\Sigma_{u-d} = \delta g_A^{(3)} = \frac{2}{3}\delta_g \cdot \tilde{\alpha}_s, \quad \delta L_{u-d} = -\frac{1}{3}\delta_g \cdot \tilde{\alpha}_s. \quad (15)$$

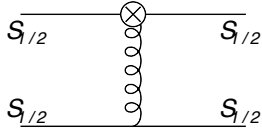
At this point our model agrees with that of Refs. [7–10]. For comparison, explicit numbers for the singlet and non-singlet contributions to the nucleon spin in the MIT bag model, as well as the OGE-improved MIT bag and cloudy

Table 3. Spin structure of the nucleon in the MIT bag model, with corrections from one-gluon exchanges (OGE), from the pion cloud and from center-of-mass rescaling. The non-gauge-invariant decomposition of the nucleon spin, Eqs. (3), is used here.

	$\Delta\Sigma/2$	L_q	$\Delta\Sigma_{u-d}/2$	L_{u-d}
relativistic (MIT bag model)	0.33	0.17	0.54	0.29
+OGE ($\tilde{\alpha}_s=1.0$):	0.30	0.20	0.55	0.28
($\tilde{\alpha}_s=2.2$):	0.27	0.23	0.56	0.27
+pion cloud ($R = 1\text{fm}$, $\tilde{\alpha}_s=1.0$):	0.24	0.26	0.51	0.26
($R = 1\text{fm}$, $\tilde{\alpha}_s=2.2$):	0.22	0.28	0.52	0.25
+center of mass ($R = 1\text{fm}$, $\tilde{\alpha}_s=1.0$):	0.30	0.20	0.64	0.20
($R = 1\text{fm}$, $\tilde{\alpha}_s=2.2$):	0.27	0.23	0.64	0.21

Table 4. Spin structure of the nucleon, based on manifestly gauge invariant operators, in the MIT bag model, together with corrections from one gluon exchanges (OGE) and from the pion cloud.

	$\Delta\Sigma/2$	L_q^{GI}	J_g^{GI}	$\Delta\Sigma_{u-d}/2$	L_{u-d}^{GI}
relativistic (MIT bag model)	0.33	0.17	0	0.54	0.29
+OGE ($\tilde{\alpha}_s=1.0$):	0.30	0.40	-0.20	0.55	0.21
($\tilde{\alpha}_s=2.2$):	0.27	0.68	-0.45	0.56	0.12
+pion cloud ($R = 1\text{fm}$, $\tilde{\alpha}_s=1.0$):	0.24	0.42	-0.16	0.51	0.19
($R = 1\text{fm}$, $\tilde{\alpha}_s=2.2$):	0.22	0.64	-0.36	0.52	0.10

**Figure 6.** One-gluon exchange diagram attached to a quark-quark-gluon interaction vertex.

Furthermore, from the gauge-invariant spin sum rule Eq. (4), we conclude that the contribution from the total gluon angular momentum equals

$$J_g^{\text{GI}} = -\delta L_{q,A}. \quad (18)$$

bag model, for two different values of $\tilde{\alpha}_s$, are displayed in Table 3.⁴

Once explicit gluon degrees of freedom, e.g. in form of one gluon exchange processes, are taken into account, questions of gauge invariance of the calculation must be carefully addressed. For a consistent calculation that includes gluon exchange contributions at order $\tilde{\alpha}_s$, and for a meaningful comparison with results from lattice QCD, we have to employ the gauge-invariant orbital angular momentum operator L_q^{GI} in Eq. (4) instead of L_q defined in (3). The covariant derivative in L_q^{GI} produces an additional quark-gluon interaction so that one must take into account the diagram in Fig. 6 for the corrections at order $\tilde{\alpha}_s$ to the MIT bag expectation values. This diagram yields the large contribution

$$\delta L_{q,A} = 0.203 \tilde{\alpha}_s, \quad (16)$$

where the subscript A stands for the gauge field interaction term. The total correction to the quark orbital momentum is then given by $\delta L_q^{\text{GI}} = \delta L_q + \delta L_{q,A}$. The diagram in Fig. 6 also contributes to the gauge invariant L_{u-d}^{GI} and shifts it by

$$\delta L_{u-d,A} = -\frac{1}{3} \delta L_{q,A}. \quad (17)$$

We notice that the corrections (16)-(18) are much larger than the known one-gluon exchange contributions from the diagrams of Fig. 5 given in Eqs. (14), (15). In particular, $\delta L_{q,A}$ dominates L_q^{MIT} for the chosen parameters. The MIT bag model results for the gauge invariant decomposition of the nucleon spin are summarized in Table 4, together with the combined results, including relativistic effects plus one-gluon exchange corrections plus corrections from the pion cloud.

To conclude this section, we emphasize that a direct calculation of $J_g^{\text{GI}} = \langle P+ | \int d^3r [\mathbf{r} \times (\mathbf{E} \times \mathbf{B})]_3 | P+ \rangle$ (i.e. not invoking the spin sum rule) in the framework of the model requires a careful treatment of the boundary conditions for the color electric fields. The boundary conditions $\hat{r} \cdot \mathbf{E}|_{r=R}$ cannot be fulfilled for the color electric fields, in the way described in [51]. This leads to a non-vanishing surface term in the calculation of J_g^{GI} and, therefore, potentially to inconsistencies with respect to the spin sum rule. A calculation with color electric fields that obey the boundary conditions, as given in [52], turns out to be significantly more involved and will not be described in this work. Note, however, that $\delta L_{q,A}$ is not affected by such complications since the corresponding operator does not involve color electric fields. It is therefore legitimate to extract the corresponding gluon angular momentum from $J_g^{\text{GI}} = 1/2 - J_q^{\text{GI}} = -\delta L_{q,A}$.

When J_g^{GI} is calculated directly, using the “wrong” color electric fields, it spoils the spin sum rule. Actually the direct evaluation of J_g^{GI} can be used to check our result

⁴ We tabulate these results here only for historical reasons as they are based on the non-gauge-invariant decomposition, Eq. (3).

for $\delta L_{q,A}$. Consider the decomposition

$$\begin{aligned} \int d^3x \mathbf{x} \times (\mathbf{E} \times \mathbf{B}) &= \int d^3x \mathbf{E} \times \mathbf{A} + \int d^3x E^i (\mathbf{x} \times \nabla) A^i \\ &- \int d^3x g \psi^\dagger (\mathbf{x} \times \mathbf{A}) \psi - \int d^3x \nabla^j [E^j (\mathbf{x} \times \mathbf{A})]. \end{aligned} \quad (19)$$

The left hand side corresponds to J_q^{GI} , the right hand side to $\Delta G + L_g - \delta L_{q,A}$ supplemented by a surface term, $-\int d^3x \nabla^j [E^j (\mathbf{x} \times \mathbf{A})]$. This surface term vanishes in the free field theory but in our model calculation this is not the case. Therefore, the total gluon angular momentum calculated through the spin sum rule equals $\int d^3x \mathbf{x} \times (\mathbf{E} \times \mathbf{B}) + \int d^3x \nabla^j [E^j (\mathbf{x} \times \mathbf{A})]$, which indeed can be confirmed by a direct calculation. In fact, the OGE corrections to ΔG and L_g cancel each other.

4 Discussion and summary

The present study has been motivated by the observation of an apparent contradiction between quark orbital angular momentum contributions, L_q and L_{u-d} , calculated in models and derived from lattice QCD computations. At the same time, model and lattice QCD results for the quark spin contributions $\Delta\Sigma$ and $g_A = \Delta\Sigma_{u-d}$ are reasonably consistent once pion cloud and gluon exchange effects are incorporated in the model [7]. When comparing the two approaches, it is essential to note that all spin observables, except g_A , are scale (and scheme) dependent quantities. Since the model scales are typically low, $\mu^2 \sim 0.1 - 0.3 \text{ GeV}^2$, a careful study of the scale evolution is necessary. In contrast to previous studies [8], our investigations are based on a “downwards” evolution of the lattice results, starting at higher scales where a perturbative treatment appears safe, to low (model) scales where higher-order effects must be taken into account. By considering the evolution at LO, NLO and NNLO, together with the possibility that the (non-perturbative) strong coupling saturates at very low scales, this approach allows us to perform a meaningful comparison of the lattice results and the spin contributions obtained in different model approaches.

With the comparatively low value of $\Lambda_{\text{QCD}}^{\text{LO}, n_F=3} = 0.148 \text{ GeV}$ obtained from the flavor matching procedure, the LO evolution is rather flat for all observables down to scales of $\mu^2 = 0.1 \text{ GeV}^2$. At this stage it is not possible to resolve the aforementioned contradiction between phenomenological or lattice results and the model results from Table 3. This is in contrast to the observation in Ref. [8].

Extending the evolution equations to NLO and NNLO, one finds a strong μ^2 -dependence at typical model scales. Even if the matching scale μ_{model}^2 is too small to draw quantitative conclusions, the trends are indicative. Employing different values for $\Lambda_{\text{QCD}}^{\text{NLO}, n_F=3}$ and $\Lambda_{\text{QCD}}^{\text{NNLO}, n_F=3}$ as obtained from flavor matching, the NLO and NNLO results for J_g , as well as for L_{u-d} , show very good overlap even at the lowest scales. For $\Delta\Sigma$ and L_q , the results at NLO and NNLO are still quantitatively comparable in

magnitude down to scales of about $\mu^2 \sim 0.3 \text{ GeV}^2$, but show larger deviations as $\mu^2 \rightarrow 0.1 \text{ GeV}^2$. In the region of such low scales where the evolution effects become strong, there is indeed an overlap with typical model results for the individual observables, as given in Table 3 and 4.

Incidentally, the NLO evolved lattice results for $\Delta\Sigma$, L_q and L_{u-d} turn out to be reasonably close to the original MIT bag values at a scale of $\mu_{\text{model}}^2 \sim 0.28 \text{ GeV}^2$ where the total contribution from the gluons vanishes, $J_g(\mu_{\text{model}}^2) = 1/2 - L_q - \Delta\Sigma/2 \simeq 0$. As the model calculations are improved, however, this apparent consistency deteriorates. Inclusion of the pion cloud in the CBM lowers $\Delta\Sigma$ and increases L_q significantly. The inclusion of the phenomenologically center of mass correction, which is not based on solid theory, would in part restore the agreement. On the other hand, inclusion of further gluon exchange corrections as in Table 4 would make the matching with the evolved lattice data at a common low scale progressively more difficult. For example, while model improvements lead to a significantly larger L_q^{GI} , thereby implying a lower matching scale, the corresponding results for the isovector L_{u-d}^{GI} become successively smaller, which would in turn require a matching at an increasingly higher scale.

It might seem that the scale dependence of $\Delta\Sigma$ implies a large gluon spin fraction ΔG at the scales of polarized DIS, larger in magnitude than the constraints provided by the HERMES, COMPASS and RHIC measurements [5, 20–22]. As a test we performed the NLO evolution downward starting from $\Delta G = 0$ at $\mu^2 = 4 \text{ GeV}^2$. One then finds $\Delta G \sim -0.4$ around the scale where J_g vanishes.

Concerning the lattice calculations, one source of systematic uncertainty can be eliminated by studying isovector quantities such as L_{u-d} for which disconnected diagrams, not taken into account in Ref. [35], cancel out. From the model investigations (see Tables 3, 4) one expects $L_{u-d}^{(GI)}$ in the range of $0.1 - 0.3$.⁵ In contrast, the lattice results start negative at $\mu^2 \sim 4 \text{ GeV}^2$. We find that the downward QCD evolution does indeed predict the appropriate change of sign (see Fig. 1d) at NLO and NNLO. Other systematic uncertainties on the lattice side, for example those related to lattice operator renormalization issues, would affect the normalization of L_{u-d} but would not change this picture significantly. As already noted above, and in contrast to the singlet L_q , inclusion of explicit gluon degrees of freedom in the properly gauge invariant treatment of the quark orbital momentum operator leads to a reduction of L_{u-d} at model scales (see Tables 3, 4) and moves this quantity closer to the extrapolated lattice QCD results. The sign change of L_{u-d} can be traced in detail by examining the crossing of L_u and L_d as shown in Fig. 2.

In summary, our analysis underlines the difficulty of a simultaneous, quantitative understanding of model calculations and lattice QCD results for the decomposition of

⁵ Note, however, that a recent calculation using a chiral quark soliton model gives a negative L_{u-d} even at low scales [53].

the nucleon's spin into the angular momenta of the constituents. While the perturbative corrections from NLO to NNLO for the evolved lattice results are at a tolerable level, the broad bands we obtain for a non-perturbative, saturated α_s indicate potentially large systematic uncertainties in the evolution at very low scales. On the side of the model calculation, we find that the effects from different types of improvements (related to the pion cloud effects, manifestly gauge invariant OAM operators, one-gluon exchange corrections) tend to make it increasingly difficult to find a common low matching scale where at least a semi-quantitative agreement with the evolved lattice results can be achieved for all of the different spin observables. Conversely, this indicates that it will be difficult to arrive at quantitatively reliable predictions from model calculations starting at scales smaller than $\mu^2 \sim 0.3 \text{ GeV}^2$ and evolving upward to scales accessible in experiments and related QCD phenomenology. We stress that this observation is not in contradiction with the phenomenologically very successful approach of "dynamically generated" (unpolarized) parton distributions (PDF) [54–56], where specific ansätze for the x -dependent PDFs are evolved from a very low initial scale, $\mu_0 < 1 \text{ GeV}$, to higher scales. The latter approach necessarily involves adjustable parameters (for each type of PDF) to achieve a fully quantitative description of the experimental DIS data at scales $Q^2 = \mu^2 > 1 \text{ GeV}^2$ and over a wide range of the momentum fractions x .

A possible exception concerning the previous critical assessment is the isovector orbital angular momentum combination L_{u-d} for which systematic lattice errors are minimal. This quantity displays generic behavior with a sign change as it evolves from lattice QCD to low scales, in accordance with the model expectations listed in Tables 3 and 4. The stability of this evolution, as one proceeds from NLO to NNLO, becomes particularly apparent when plotted as a function of α_s and compared with the corresponding evolution of the average momentum fraction, $\langle x \rangle_{u-d}$.

Acknowledgments

It is a pleasure to thank Werner Vogelsang, Markus Diehl, and Marek Karliner for helpful discussions. This work has been partially supported by BMBF, GSI, and by the DFG cluster of excellence "Origin and Structure of the Universe". MA and PH gratefully acknowledge the support by the Emmy-Noether program of the DFG. PH is supported by the SFB/TRR-55 of the DFG. EMH thanks Wolfram Weise for his hospitality and the A. v. Humboldt Foundation for a (month-long) stay at the Technische Universität München.

References

1. J. Ashman *et al.* [European Muon Collaboration], Phys. Lett. B **206** (1988) 364.
2. A. Airapetian *et al.* [HERMES Collaboration], Phys. Rev. D **75** (2007) 012007 [arXiv:hep-ex/0609039].
3. V. Y. Alexakhin *et al.* [COMPASS Collaboration], Phys. Lett. B **647**, 8 (2007) [arXiv:hep-ex/0609038].
4. J. Blümlein, H. Böttcher, Nucl. Phys. B **841** (2010) 205–230. [arXiv:1005.3113 [hep-ph]].
5. D. de Florian, R. Sassot, M. Stratmann and W. Vogelsang, Phys. Rev. D **80** (2009) 034030 [arXiv:0904.3821 [hep-ph]].
6. E. Leader, A. V. Sidorov and D. B. Stamenov, arXiv:1010.0574 [hep-ph].
7. F. Myhrer and A. W. Thomas, Phys. Lett. B **663** (2008) 302 [arXiv:0709.4067 [hep-ph]].
8. A. W. Thomas, Phys. Rev. Lett. **101** (2008) 102003 [arXiv:0803.2775 [hep-ph]].
9. A. W. Thomas, Int. J. Mod. Phys. E **18** (2009) 1116 [arXiv:0904.1735 [hep-ph]].
10. A. W. Thomas, Prog. Part. Nucl. Phys. **61** (2008) 219 [arXiv:0805.4437 [hep-ph]].
11. P. Hägler, J. W. Negele, D. B. Renner, W. Schroers, T. Lipert, K. Schilling [LHPC collaboration and SESAM collaboration], Phys. Rev. D **68**, 034505 (2003) [arXiv:hep-lat/0304018].
12. M. Göckeler, R. Horsley, D. Pleiter, P. E. L. Rakow, A. Schäfer, G. Schierholz and W. Schroers [QCDSF Collaboration], Phys. Rev. Lett. **92**, 042002 (2004) [arXiv:hep-ph/0304249].
13. Ph. Hägler *et al.* [LHPC Collaborations], Phys. Rev. D **77** (2008) 094502 [arXiv:0705.4295 [hep-lat]].
14. R. L. Jaffe and A. Manohar, Nucl. Phys. B **337**, 509 (1990).
15. X. D. Ji, J. Tang and P. Hoodbhoy, Phys. Rev. Lett. **76** (1996) 740 [arXiv:hep-ph/9510304].
16. X. D. Ji, Phys. Rev. Lett. **78** (1997) 610 [arXiv:hep-ph/9603249].
17. M. Burkardt, A. Miller and W. D. Nowak, Rept. Prog. Phys. **73**, 016201 (2010) [arXiv:0812.2208 [hep-ph]].
18. M. Wakamatsu, Phys. Rev. D **81**, 114010 (2010) [arXiv:1004.0268 [hep-ph]].
19. R. L. Jaffe, Phys. Lett. B **365**, 359 (1996) [arXiv:hep-ph/9509279].
20. M. Alekseev *et al.* [COMPASS Collaboration], Phys. Lett. B **676** (2009) 31 [arXiv:0904.3209 [hep-ex]].
21. A. Airapetian *et al.* [HERMES Collaboration], arXiv:1002.3921 [hep-ex].
22. B. I. Abelev *et al.* [STAR Collaboration], Phys. Rev. Lett. **100** (2008) 232003. [arXiv:0710.2048 [hep-ex]].
23. A. J. Buras, Rev. Mod. Phys. **52** (1980) 199.
24. E. G. Floratos, D. A. Ross and C. T. Sachrajda, Nucl. Phys. B **152** (1979) 493.
25. S. A. Larin, T. van Ritbergen, J. A. M. Vermaseren, Nucl. Phys. B **427** (1994) 41–52.
26. S. A. Larin, P. Nogueira, T. van Ritbergen *et al.*, Nucl. Phys. B **492** (1997) 338–378. [hep-ph/9605317].
27. A. Retey and J. A. M. Vermaseren, Nucl. Phys. B **604** (2001) 281 [arXiv:hep-ph/0007294].
28. M. Wakamatsu and Y. Nakakoji, Phys. Rev. D **77** (2008) 074011 [arXiv:0712.2079 [hep-ph]].
29. G. 't Hooft, Nucl. Phys. B **61** (1973) 455.
30. W. A. Bardeen, A. J. Buras, D. W. Duke and T. Muta, Phys. Rev. D **18** (1978) 3998.
31. R. Mertig and W. L. van Neerven, Z. Phys. C **70** (1996) 637 [arXiv:hep-ph/9506451].
32. W. Vogelsang, Phys. Rev. D **54** (1996) 2023 [arXiv:hep-ph/9512218].

33. A. Vogt, S. Moch, M. Rogal and J. A. M. Vermaseren, Nucl. Phys. Proc. Suppl. **183** (2008) 155 [arXiv:0807.1238 [hep-ph]].
34. Ph. Hägler, Phys. Rept. **490**, 49 (2010) [arXiv:0912.5483 [hep-lat]].
35. J. D. Bratt *et al.* [LHPC Collaboration], Phys. Rev. **D82** (2010) 094502. [arXiv:1001.3620 [hep-lat]].
36. M. Dorati, T. A. Gail and T. R. Hemmert, Nucl. Phys. A **798**, 96 (2008) [arXiv:nucl-th/0703073].
37. S. D. Bass, A. W. Thomas, Phys. Lett. **B684** (2010) 216-220. [arXiv:0912.1765 [hep-ph]], and refs. therein.
38. K. Nakamura *et al.* [Particle Data Group Collaboration], J. Phys. G **G37** (2010) 075021.
39. S. Bethke, Eur. Phys. J. **C64** (2009) 689-703. [arXiv:0908.1135 [hep-ph]].
40. K. G. Chetyrkin, B. A. Kniehl, M. Steinhauser, Phys. Rev. Lett. **79** (1997) 2184-2187. [hep-ph/9706430].
41. D. V. Shirkov and I. L. Solovtsov, Phys. Rev. Lett. **79** (1997) 1209 [arXiv:hep-ph/9704333].
42. C. S. Fischer, R. Alkofer, Phys. Rev. **D67** (2003) 094020. [hep-ph/0301094].
43. G. M. Prosperi, M. Raciti, C. Simolo, Prog. Part. Nucl. Phys. **58**, 387-438 (2007). [hep-ph/0607209].
44. A. W. Thomas and W. Weise, "The Structure of the Nucleon," *Berlin, Germany: Wiley-VCH (2001) 389 p*
45. A. W. Thomas, Adv. Nucl. Phys. **13** (1984) 1.
46. S. Theberge and A. W. Thomas, Nucl. Phys. A **393** (1983) 252.
47. A. Chodos, R. L. Jaffe, K. Johnson and C. B. Thorn, Phys. Rev. D **10** (1974) 2599.
48. T. A. DeGrand, R. L. Jaffe, K. Johnson and J. E. Kiskis, Phys. Rev. D **12** (1975) 2060.
49. M. Schumann, R. J. Lindebaum and R. D. Viollier, Eur. Phys. J. C **16** (2000) 331.
50. H. Hogaasen and F. Myhrer, Phys. Rev. D **37** (1988) 1950.
51. J. Wroldsen and F. Myhrer, Z. Phys. C **25** (1984) 59.
52. R. D. Viollier, S. A. Chin and A. K. Kerman, Nucl. Phys. A **407** (1983) 269.
53. M. Wakamatsu, Eur. Phys. J. A **44** (2010) 297 [arXiv:0908.0972 [hep-ph]].
54. M. Gluck, E. Reya and A. Vogt, Z. Phys. C **67**, 433 (1995).
55. M. Gluck, E. Reya and A. Vogt, Eur. Phys. J. C **5**, 461 (1998) [arXiv:hep-ph/9806404].
56. P. Jimenez-Delgado and E. Reya, Phys. Rev. D **79**, 074023 (2009) [arXiv:0810.4274 [hep-ph]].